Ab Initio Molecular Dynamics Study on the Electron Capture Processes of Protonated Methane (CH_5^+)

Hiroto Tachikawa*,† and Andrew J. Orr-Ewing*,‡

Division of Materials Chemistry, Graduate School of Engineering, Hokkaido University, Sapporo 060-8628, Japan, and School of Chemistry, University of Bristol, Bristol BS8 1TS, U.K.

Received: July 10, 2008; Revised Manuscript Received: September 29, 2008

Electron capture dynamics of protonated methane (CH_5^+) have been investigated by means of a direct ab initio molecular dynamics (MD) method. First, the ground and two low-lying state structures of CH_5^+ with eclipsed C_s, staggered C_s and C_{2v} symmetries were examined as initial geometries in the dynamics calculation. Next, the initial structures of CH_5^+ in the Franck−Condon (FC) region were generated by inclusion of zero point energy and then trajectories were run from the selected points on the assumption of vertical electron capture. Two competing reaction channels were observed: $CH_5^+ + e^- \rightarrow CH_4 + H$ (I) and $CH_5^+ + e^- \rightarrow CH_3 + H_2$ (II). Channel II occurred only from structures very close to the s-C_s geometry for which two protons with longer C−H distances are electronically equivalent in CH_5^+. These protons have the highest spin density as hydrogen atoms following vertical electron capture of CH_5^+ and are lost as H_2. On the other hand, channel I was formed from a wide structural region of CH_5^+. The mechanism of the electron capture dynamics of CH_5 is discussed on the basis of the theoretical results.

1. Introduction

Electron capture by protonated alkanes, RH_2^+, is among the most important chemical processes that occur in radiation chemistry.[1,2] The γ-ray irradiation of neat alkanes (RH) causes ionization of RH, forming an electron and a radical cation (RH^+):

$$RH + h\nu \rightarrow RH^+ + e^- \quad (1)$$

The radical cation RH^+ reacts easily with a neutral alkane (RH):

$$RH^+ + RH \rightarrow RH_2^+ + R \quad (2)$$

by proton transfer reaction, forming a protonated alkane (RH_2^+) and neutral radical (R). Of the possible decay pathways of RH_2^+, electron capture reactions are the most significant, and are expressed by

$$RH_2^+ + e^- \rightarrow [RH_2] \rightarrow RH + H \quad (3)$$

$$\rightarrow R + H_2 \quad (4)$$

Protonated methane, CH_5^+, is the simplest protonated alkane and has a highly fluxional character.[3−18] The most stable equilibrium structure of CH_5^+, i.e., the global minimum on the potential energy surface (PES) within the Born−Oppenheimer approximation, is an eclipsed C_s structure in which an H_2 moiety is attached in an eclipsed orientation with respect to the CH_3^+ moiety. The neutralization of CH_5^+ and related ions by dissociative recombination with a free electron is considered likely to be of importance in astrophysics.[5,6,18] Recently, Mann et al.[18] observed the electron capture reaction of protonated methane ions CH_5^+ in the gas phase and measured kinetic energy release (KER) distributions of the products formed from the reaction. They found two sets of reaction products:

$$CH_5^+ + e^- \rightarrow [CH_5]_{ver} \rightarrow CH_4 + H \quad (I)$$

$$\rightarrow CH_3 + H_2 \quad (II)$$

where $[CH_5]_{ver}$ means a CH_5 radical at the vertical electron capture point of CH_5^+. The KERs in both channels were distributed from zero to 4.5 eV, with peaks at 3.0 eV, and the KER distribution of channel II was bimodal. The reaction dynamics of CH_5 were also investigated by running quasi-classical trajectory (QCT) calculations using a PES obtained by ab initio calculation. The QCT calculation outcomes showed that reaction channels I and II are competitive, but that channel II is minor. In these calculations, first, an ab initio-based global PES for $H + CH_4$ that describes the abstraction and exchange reactions $H + CH_4 \rightarrow H_2 + CH_3$ and $H + CH_4 \rightarrow CH_4 + H$ was calculated, and then the energies were fit to a polynomial function.[19,20] Full dimensionality ab initio molecular dynamics (MD) calculations for CH_5 without this fitting provide an alternative method for exploring the nature of the dissociation dynamics. As we show here, these calculations provide further insights about the structures and electronic character of $[CH_5]_{ver}$ (formed by electron attachment to the various geometries of CH_5^+) that lead to fragmentation via the two competing pathways.

Ab initio and molecular dynamics methods of the type employed here were used previously by Hickman et al. to investigate the electron capture reaction of $HCNH^+$ (i.e., $HCNH^+ + e^-$).[21] Rates for dissociative recombination, a process of importance (along with other electron capture reactions of molecular ions) in the interstellar medium, breaking either the CH bond or the NH bond (leading to HNC + H and HCN + H, respectively), were calculated using a simple quasi-diatomic model. Similar calculations have been carried out by one of us.[22] These investigations suggest that full-dimensional direct ab initio MD is an important tool to explore the reaction dynamics of such systems.

In the present calculation, a direct ab initio MD method is applied to the dynamics following electron capture by the protonated methane ion CH_5^+. We do not restrict the dimensions of the PES in the calculations of the subsequent reaction

* Author for correspondence. E-mail: hiroto@eng.hokudai.ac.jp.
† Hokkaido University.
‡ University of Bristol.

10.1021/jp806114y CCC: $40.75
Published on Web 10/29/2008

dynamics of CH_5. As a result, further interesting details of the dissociation dynamics are obtained.

2. Computational Methods

The structures of CH_5^+ were fully optimized at the MP2/6-311++G(d,p) level of theory. Previous theoretical calculations showed that, within the Born−Oppenheimer approximation, CH_5^+ has three low-energy stationary points with eclipsed-C_s, staggered-C_s and C_{2v} symmetries.[4,8−17] The energies of these structures lie close to each other. The electron capture dynamics calculations were therefore first carried out from these stationary points. Next, the geometries of CH_5^+ were randomly generated by inclusion of zero point energy (ZPE) to allow for the fluxional nature of the ion and trajectories for the neutral radical CH_5 were run from these generated points on the assumption of vertical electron capture (i.e., the Franck−Condon approximation). The electronic state of the system was monitored during the simulation. We confirmed carefully that the electronic state is maintained during the reaction and thus considered dynamics only on the ground-state PES of the CH_5 system.

The velocities of atoms at the starting point were set to zero (i.e., the momentum vector of each atom is zero). The equations of motion for N atoms in a molecule are given by

$$\frac{dQ_j}{dt} = \frac{\partial H}{\partial P_j} \tag{5}$$

$$\frac{dP_j}{dt} = -\frac{\partial H}{\partial Q_j} = -\frac{\partial U}{\partial Q_j} \tag{6}$$

where $j = 1 - 3N$, H is the classical Hamiltonian, Q_j is the Cartesian coordinate of the jth mode and P_j is the conjugate momentum. These equations were numerically solved by the velocity Verlet algorithm method. No symmetry restrictions were applied to the calculation of the energy gradients. The time step size was chosen as 0.10 fs, and a total of 10000 or 20000 steps were calculated for each dynamics calculation. The drift of the total energy is confirmed to be less than 10^{-3}% throughout all steps in the trajectory. The momentum of the center of mass and the angular momentum were set to zero. The total energy of the system (4.7 eV, 108 kcal mol^{-1}) was fixed to the sum of the zero-point energy of CH_5^+, and the available energy of $[CH_5]_{ver}$ (the energy difference between $[CH_5]_{ver}$ and the products is calculated to be 3.3 eV at the MP2/6-311++G(d,p) level). The total energy is comparable to the 4.1 eV available in the electron capture experiments of Mann et al.[18] but is much less than the energies for experimental studies of the dissociative recombination (DR) of CH_5^+, which exceed 8 eV.[6] Further details of the direct MD calculations are described elsewhere.[22−26]

Static ab initio calculations were carried out using Gaussian 03.[27] To confirm the stability of the complexes at all stationary points, harmonic vibrational frequencies were calculated at the MP2/6-311++G(d,p) level of theory. The relative energies were also calculated at the MP4SDQ, CCSD, and QCISD/6-311++G(d,p) levels of theory for comparison. Results are also compared, where appropriate, with prior calculations of the structures and energetics of the CH_5^+ and CH_5 systems.[4,8−20]

3. Results

A. Structures and Electronic States of CH_5^+ and CH_5. ***Eclipsed-C_s.*** First, the structure of CH_5^+(e-C_s) with eclipsed C_s symmetry (denoted by e-C_s) was optimized at the MP2/6-311++G(d,p) level of theory. The optimized structure is given in Figure 1, with parameters also summarized in Table 1. The

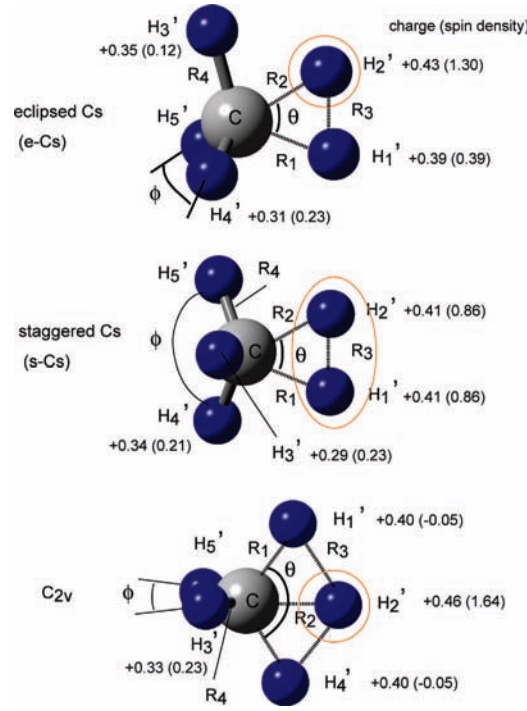

Figure 1. Optimized structures and geometrical parameters of CH_5^+ calculated at the MP2/6-311++G(d,p) level. Three structures of CH_5^+, denoted as eclipsed (e-C_s), staggered (s-C_s), and C_{2v} are shown and discussed further in the text. The values indicate NPA charges of CH_5^+ and spin densities of the CH_5 radical (in parenthesis) at the equivalent geometries.

TABLE 1: Optimized Geometrical Parameters for CH_5^+ with e-C_s, s-C_s and C_{2v} Symmetries Calculated at the MP2/6-311++G(d,p) level (Bond Lengths and Angles in Å and degrees, Respectively)

	e-C_s	s-C_s	C_{2v}
$r(C-H_1') = R_1$	1.1862	1.2087	1.1407
$r(C'-H_2') = R_2$	1.1890	1.2087	1.1634
$r(H_1' - H_2') = R_3$	0.9754	0.9619	1.1783
$r(C-H_3') = R_4$	1.1107	1.0851	1.0879
$r(C-H_4')$	1.0889	1.1007	1.0882
$r(C-H_5')$	1.0889	1.1007	1.0882
θ	48.5	45.4	123.2
ϕ	119.9	106.6	122.0
E/au	−40.5908291	−40.5905942	−40.5899841

bond distances of the C−H and H−H were calculated to be $R_1 = 1.186$, $R_2 = 1.189$, R_3 (=$r(H_1'-H_2')$) = 0.975, $R_4 = r(C-H_3')$ = 1.111, and $r(C-H_4') = r(C-H_5') = 1.089$ Å. The distances of two of the H atoms from the carbon atom are slightly longer than the others. The atomic charges on the H atoms of CH_5^+ were calculated by means of natural population analysis (NPA) and were obtained as $H_1' = +0.39$, $H_2' = +0.43$, $H_3' = +0.35$ and H_4' (=H_5') = +0.31 (with the C atom carrying a net negative charge). Thus, the positive charges are almost equivalently distributed on all the H atoms, with only small differences. This result indicates that the H atoms in this geometry of CH_5^+ are almost equivalent, although the positive charge of one atom (H_2') is slightly larger than the others. The geometries (and those calculated for the s-C_s and C_{2v} structures discussed below) agree well with the previously published structures of Brown et al. computed at the MP2/cc-pVTZ level of theory.[12,13] For example, these authors reported the following bond distances for C−H and H−H in the e-C_s structure: $R_1 = 1.180$, $R_2 = 1.183$, and R_3 = 0.976 Å.

The electronic states of $[CH_5]_{ver}$ were calculated at the MP2/6-311++G(d,p) level, where, as noted earlier, $[CH_5]_{ver}$ indicates a CH_5 radical with geometry corresponding to the CH_5^+ at the electron capture point (i.e., the result of a vertical electron capture process). The spin densities of hydrogen atoms of $[CH_5]_{ver}$ are given in Figure 1. The spin densities on H_1', H_2', H_3' and H_4' (=H_5') are calculated to be 0.39, 1.30, 0.12, and 0.23, respectively, indicating that the spin density is largely localized on only one hydrogen atom (H_2'). This feature is not dependent on the level of theory employed in the calculation (see Supporting Information). As will be shown in a later section, the hydrogen atom possessing a large spin density (i.e., the H_2' atom) is preferentially dissociated after electron capture by CH_5^+.

Staggered-C_s. The structure of CH_5^+ with a staggered form, denoted by s-C_s, is given in the middle panel of Figure 1. Two hydrogen atoms (H_1' and H_2') are equivalent, and the C−H bond distances (C−H_1' and C−H_2') are significantly longer than those of the other bonds (1.209 vs 1.100 Å). The charges on H_1' (=H_2'), H_3', and H_4' (=H_5') atoms are calculated to be +0.41, +0.29, and +0.34, respectively. The positive charges are nearly evenly distributed over all H atoms, much as seen for CH_5^+(e-C_s).

The spin densities at the vertical electron capture point of CH_5^+(s-C_s) are calculated to be $H_1' = H_2' = 0.86$, $H_3' = 0.23$, $H_4' = H_5' = 0.21$, indicating that two hydrogen atoms (H_1' and H_2') have large and equivalent spin density. This result suggests that $[CH_5(s\text{-}C_s)]_{ver}$ is composed of a methyl radical and two hydrogen atoms, expressed by CH_3--H--H. This deduction is not dependent on the level of theory (see Supporting Information). A hydrogen molecule (H_1'−H_2') dissociates from CH_5^+(s-C_s) after electron capture via this geometry.

C_{2v}. Previous theoretical studies showed that CH_5^+ also has a stationary point corresponding to a C_{2v} symmetry geometry. The optimized structure of $CH_5^+(C_{2v})$ is illustrated in the bottom panel of Figure 1. One atom (H_2') is located along the C_2 axis of the CH_4. The atomic charges on the H_1', H_2', H_3' (=H_5'), and H_4' atoms are +0.40, +0.46, +0.33, and +0.40, respectively, indicating that the positive charge is delocalized widely over CH_5^+, although H_2' has a slightly larger value. The C_{2v} structure has a slightly higher sum of NPA charges on the H atoms than for the C_s structures, indicating a greater degree of charge separation. Spin densities for neutral $[CH_5(C_{2v})]_{ver}$ were calculated to be $H_1' = -0.05$, $H_2' = 1.64$, H_3' (=H_5') = 0.23, and $H_4' = -0.05$. This result indicates that the spin density is only localized on the H_2' atom of $[CH_5(C_{2v})]_{ver}$. From this geometry, a hydrogen atom (H_2') is dissociated after electron capture.

Harmonic Vibrational Frequency. Harmonic vibrational frequencies of CH_5^+ with e-C_s, s-C_s and C_{2v} symmetries were calculated at the MP2 level. The results are summarized in Table S1 in the Supporting Information. The CH_5^+(s-C_s) ion has all real frequencies, whereas s-C_s and C_{2v} structures have an imaginary frequency. These results indicate that CH_5^+(e-C_s) is located in a minimum (in this case, the global minimum) of the ground-state PES, whereas s-C_s and C_{2v} geometries correspond to transition states. The zero-point energies and an imaginary frequency of s-C_s are in reasonable agreement with the previous calculations by Brown et al. (e.g., the imaginary frequencies obtained here and reported previously are, respectively, 238i cm^{-1} and 216i cm^{-1}).[12,13] From an analysis of normal modes, CH_5^+(s-C_s) is found to be located at a saddle point for the H_2 rotation about the C_3 axis of the CH_3 moiety of CH_5^+. The C_{2v} structure corresponds to a saddle point for the structural change e-C_s → C_{2v} → e-C_s. Similar calculations were carried out at the QCISD and CCSD levels of theory, and both calculations showed that the e-C_s structure is a global minimum, while the s-C_s and C_{2v} structures are saddle points for internal structural changes (see Supporting Information). These deductions are in accord with previous calculations of the structures of stationary points on the CH_5^+ PES.[4,7−17]

TABLE 2: Relative Energies (ΔE), Zero Point Energies, and ZPE-Corrected Relative Energies (All in kcal/mol) of CH_5^+ with e-C_s, s-C_s and C_{2v} Symmetries Calculated at the MP2/6-311++G(d,p) Level[a]

	ΔE /kcal/mol	ZPE/kcal/mol	ΔE +ΔZPE/kcal/mol
e-C_s	0.0 (0.0)	32.71 (32.71)	0.0 (0.0)
s-C_s	0.15 (0.10)	32.55 (32.50)	−0.01 (−0.11)
C_{2v}	0.53 (1.12)	31.77 (31.67)	−0.41 (0.08)

[a] In each case, relative values are quoted with respect to the e-C_s Structure. Values calculated at the QCISD/6-311++G(d,p) level (in kcal/mol) are in parentheses.

TABLE 3: NPA Charges of Hydrogen Atoms in CH_5^+ and Spin Densities on Hydrogen Atoms in CH_5 at the Vertical Electron Capture Point of CH_5^+, Denoted by $[CH_5]_{ver}$[a]

	e-C_s		s-C_s		C_{2v}	
atom	charge	spin density	charge	spin density	charge	spin density
H_1	+0.39	0.39	+0.41	0.86	+0.40	−0.05
H_2	+0.43	1.30	+0.41	0.86	+0.46	1.64
H_3	+0.35	0.12	+0.29	0.23	+0.33	0.23
H_4	+0.31	0.23	+0.34	0.21	+0.40	−0.05
H_5	+0.31	0.23	+0.34	0.21	+0.33	0.23

[a] The values are calculated at the MP2/6-311++G(d,p) level of theory.

Total and relative energies are given in Table 2. The relative energies for the three structures are 0.00 kcal/mol (e-C_s), 0.15 kcal/mol (s-C_s) and 0.53 kcal/mol (C_{2v}). Brown et al. obtained energies of the s-C_s and C_{2v} structures that were, respectively, 0.12 and 0.55 kcal/mol above the e-C_s minimum.[12,13] If zero point energies are included, the relative energies from our calculations are changed to 0.00 kcal/mol (e-C_s), −0.01 kcal/mol (s-C_s) and −0.41 kcal/mol (C_{2v}). The results indicate that these structures are energetically close to each other and that there are no barriers to their interconversion.[4,7−17] The calculated electron affinities are also found to be similar: values are 99.9 kcal/mol (e-C_s and s-C_s) and 98.7 kcal/mol (C_{2v}).

To check the level of theory used in the calculations, QCISD/6-311++G(d,p) calculations were also carried out for the three stationary points. The relative energies are calculated to be 0.00 kcal/mol (e-C_s), 0.10 kcal/mol (s-C_s) and 1.12 kcal/mol (C_{2v}). After zero-point energy correction, the energies are 0.0 kcal/mol (e-C_s), −0.11 kcal/mol (s-C_s) and 0.08 kcal/mol (C_{2v}), which are very similar to the MP2 values.

Summary of Static ab Initio Calculations. In this section, we described the static ab initio calculations carried out for CH_5^+ and $[CH_5]_{ver}$ to elucidate the structures and electronic states within the Born−Oppenheimer approximation. The results for geometric parameters, energetics, charges and spin densities are summarized in Tables 1−3. As was concluded from previous theoretical studies,[4,7−17] CH_5^+(e-C_s) is located at the global minimum, while CH_5^+(s-C_s) and (C_{2v}) correspond to saddle points for internal structural deformation of CH_5^+. However, the energy differences of these structures are negligibly small. We also found that the electronic charge states of all hydrogen atoms of CH_5^+ are almost equivalent in the cationic state. On the other hand, the electronic states of the hydrogen atoms of

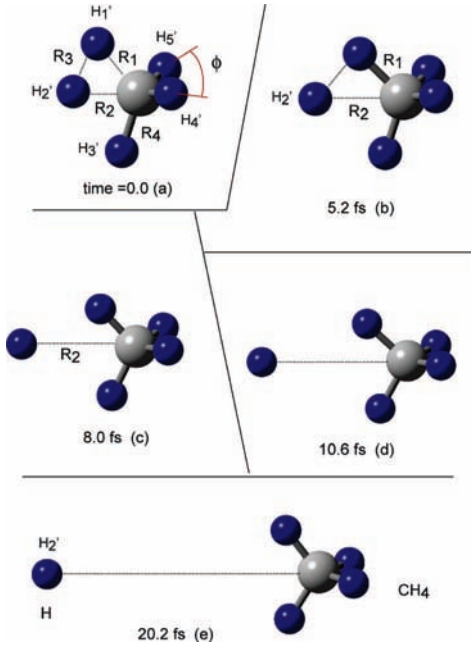

Figure 2. Snapshots along the pathway for the electron capture reaction of CH_5^+(e-C_s) obtained by direct ab initio MD calculation at the MP2/6-311++G(d,p) level. The products are CH_4 + H. No symmetry restrictions were applied in the calculations.

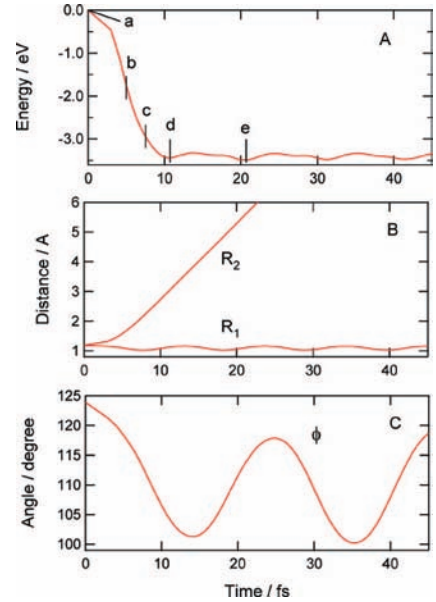

Figure 3. Time propagations of (A) potential energy, (B) distances (R_1 and R_2), and (C) angle (ϕ = H$_4$′−C−H$_5$′) for the electron capture reaction of CH_5^+(e-C_s). No symmetry restrictions were applied in the calculations. Notations (a)−(e) correspond to those of Figure 2.

CH_5^+ are drastically changed by vertical electron capture. The spin density is localized on specific hydrogen atoms of $[CH_5]_{ver}$. In e-C_s and C_{2v} geometries, the spin density is localized on one of the hydrogen atoms of $[CH_5]_{ver}$, whereas, for the s-C_s structure, the excess electron is localized equivalently on two hydrogen atoms of $[CH_5]_{ver}$.

B. Electron Capture Dynamics of CH_5^+ with e-C_s Symmetry. Having optimized the structure of CH_5^+(e-C_s) at the MP2/6-311++G(d,p) level of theory and tested the calculations against prior studies, the dynamics following the electron capture,

$$CH_5^+(\text{e-}C_s) + e^- \rightarrow [CH_5]_{ver} \rightarrow \text{product}$$

can be investigated by means of a direct ab initio MD method on the assumption of vertical electron attachment. No symmetry restrictions are imposed on the dynamics calculations.

Snapshots obtained from the calculations are illustrated in Figure 2. The C−H bond distances of CH_5(e-C_s) are R_1 = 1.186 Å and R_2 = 1.188 Å at time zero, and are slightly longer than the others (R_4 = 1.111 Å, r(C−H$_4$′) = r(C−H$_5$′) = 1.089 Å). After the electron capture, one of the hydrogen atoms (the H$_2$′ atom) is rapidly dissociated from CH_5. These dynamics continue until complete dissociation to the final products, CH_4 + H.

To obtain more quantitative features of the dissociation mechanism, the time evolution of the potential energy and the C−H bond distances are plotted in Figure 3 for the trajectory for which snapshots are shown in Figure 2. The zero of the potential energy corresponds to the energy level at the vertical electron capture point, $[CH_5]_{ver}$. After the electron capture by CH_5^+, the energy decreases suddenly as a function of time and reaches a limiting value at 10−20 fs (−3.5 eV). Thereafter, the energy oscillates slightly with time. The retention of R_1 (with some oscillation) but the elongation of R_2 is also shown; for example, the R_2(C−H$_2$′) bond distances at time 7.96 and 20.01 fs are calculated to be 2.223 and 5.299 Å, respectively. This result suggests that one of the hydrogen atoms of CH_5^+ is directly dissociated without complex formation during the electron capture reaction. The other C−H bonds vibrate rapidly around the equilibrium C−H distance of CH_4. The time dependences of R$_1$ and ϕ (see Figure 1 for a definition) show that the C−H stretching and H−C−H bending modes of the product CH_4 vibrate with frequencies 3175 and 1598 cm^{-1}, respectively. Finally, the electron capture reaction from the e-C_s geometry leads to the hydrogen atom dissociation channel (the products are CH_4 + H). The relative translational energy between CH_4 and H is calculated to be 3.22 eV, which is in good agreement with the experimental data for channel I obtained by Mann et al.[18]

C. Electron Capture Dynamics of CH_5^+ with s-C_s Symmetry. In this section, the dynamics following electron capture by CH_5^+(s-C_s) are investigated in the same manner as for CH_5^+(e-C_s). The reaction is expressed as

$$CH_5^+(\text{s-}C_s) + e^- \rightarrow [CH_5]_{ver} \rightarrow \text{products}$$

Snapshots of geometries of the CH_5 structure after the electron capture are illustrated in Figure 4. The C−H and H$_1$−H$_2$ bond distances of CH_5(s-C_s) are R_1 = 1.191 Å, R_2 = 1.191 Å, and R_3 = 0.962 Å at time zero. After the electron capture, the hydrogen molecule (H$_1$′−H$_2$′) is formed and rapidly dissociates from CH_3. The hydrogen molecule fully separates from the methyl radical, giving CH_3 + H_2 as the final products.

The time evolutions of potential energy and geometrical parameters are plotted in Figure 5. The potential energy decreases to −3.22 eV at 18.8 fs (point c) and it stabilizes around −3.2 eV. After the electron capture, two C−H bonds (R_1 and R_2) rapidly elongate as time evolves. For example, the C−H bond distances (R_1) at time 8.99 and 30.25 fs are calculated to be 1.619 and 5.424 Å, respectively. Molecular hydrogen is released after electron capture, and the relative translational energy between CH_3 and H_2 is calculated to be 3.02 eV, which agrees well with the experimental data for channel II reported by Mann et al.[18]

The H$_1$′−H$_2$′ bond distance of the product hydrogen molecule is plotted as a function of time in Figure 5 and is seen to oscillate with a time period and amplitude that are calculated to be 7.3 fs and 0.1 Å, respectively, indicating that the product H_2 is

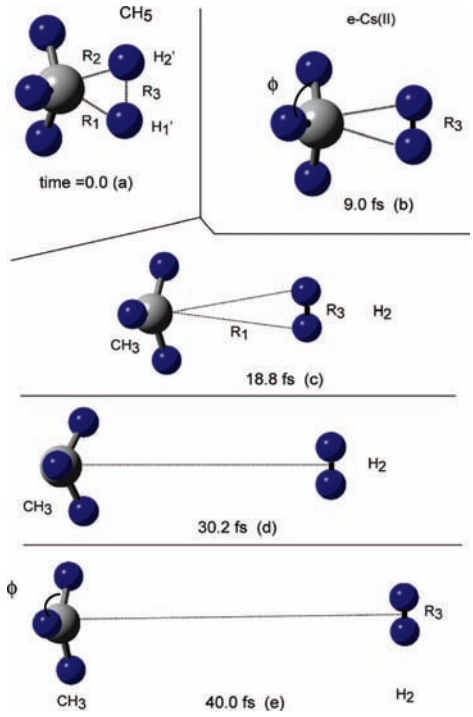

Figure 4. Snapshots for the electron capture reaction of CH_5^+(s-C_s) obtained by direct ab initio MD calculation. The products are CH_3 + H_2. No symmetry restrictions were applied in the calculations.

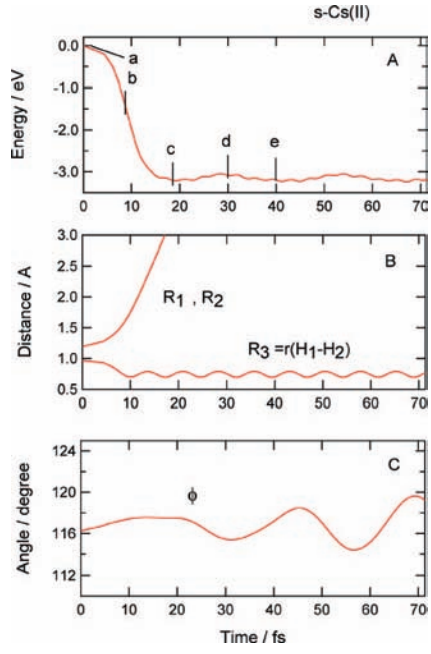

Figure 5. Time propagations of (A) potential energy, (B) distances (R_1, R_2 and R_3), and (C) angle ($\phi = H_4'-C-H_5'$) for the electron capture reaction of CH_5^+(s-C_s). No symmetry restrictions were applied in the calculations. Notations (a)−(e) correspond to those of Figure 4.

vibrationally excited. This excitation is caused by the large $H_1'-H_2'$ bond distance at time zero (0.9619 Å). The stretching mode of product H_2 vibrates with a frequency of 4550 cm^{-1} and the H−C−H bending mode of the methyl radical is observed to vibrate with a frequency of 1190 cm^{-1}.

D. Electron Capture Dynamics of CH_5^+ with C_{2v} Symmetry. The results of dynamics calculation for dynamics initiated from the $CH_5^+(C_{2v})$ geometry are given in the Supporting Information. The reaction is expressed by

$$CH_5^+(C_{2v}) + e^- \rightarrow [CH_5]_{ver} \rightarrow \text{products}$$

The C−H bond distances of $CH_5(C_{2v})$ are R_1 = 1.145 Å and R_2 = 1.163 Å at time zero. After the electron capture, one of the C−H bonds (R_2) increases gradually with time: the C−H bond distance, (R_2) for the extending bond at times 4.7, 10.1 and 19.9 fs are calculated to be 1.662, 2.999 and 5.561 Å, respectively. Thus, one of the hydrogen atoms of CH_5^+ is directly dissociated, leaving the other C−H bonds to vibrate rapidly around the equilibrium C−H distance of CH_4. The angles (θ and ϕ, see Figure 1) vibrate with time periods of 22 and 21 fs, respectively. This electron capture reaction asymptotically results in loss of a hydrogen atom, so the products are CH_4 + H. The relative translational energy of the CH_4 and H is calculated to be 3.26 eV, which is also in good agreement with experimental data.[18]

E. Effects of Zero Point Energy of CH_5^+ on the Dynamics. In an actual system, the structure of CH_5^+ fluctuates around the 120 equivalent e-C_s minima because of the ZPE. To include the fluxional nature of the ion geometry in the study of the dissociative recombination dynamics, which have so far focused on selected geometries, the geometrical configurations of CH_5^+ were randomly generated by direct ab initio MD calculation with ZPE, and then trajectories were run from the selected points.

The results of direct ab initio MD calculations of CH_5^+ with ZPE are illustrated in Figure 6. The potential energy oscillates as a function of time, and the positions of the hydrogen atoms change markedly over time as the CH_5^+ ion passes through several configurations during the simulation. The total energy (the sum of potential and kinetic energies) is constant at the ZPE (32.7 kcal/mol) level during the simulation. From the direct ab initio MD calculations with ZPE, 38 geometrical configurations were generated and electron capture dynamics calculations run from these geometries. The two channels (denoted as I and II) were observed as product channels, but only three trajectories gave channel II. The branching ratio to channels I and II (I:II) is therefore roughly estimated to be 13:1, indicating that channel II is only a minor product of the reaction, with loss of a single H atom dominating.

F. Origin of the Reaction Channels. In this section, the origins of reaction channels I and II are considered on the basis of the theoretical results. The present calculations show that the electron capture by CH_5^+ results in both channels I and II because the CH_5^+ ion adopts a variety of geometrical configurations on the ground-state PES and the hydrogen atoms of the CH_5 radical at the vertical electron capture point $[CH_5]_{ver}$ acquire specific spin densities.

Two typical structures of $[CH_5]_{ver}$ at time zero with inclusion of zero-point energy are illustrated in Figure 7. The upper and lower structures lead to channels I and II, respectively. The present direct ab initio MD calculations show that channel II occurs only from a specific geometrical configuration where the two hydrogen atoms with longer C−H bonds are equivalent and have high spin density at the start of the trajectory. In the case of the s-C_s structure, two H atoms are symmetrically equivalent, so that the $[CH_5(s\text{-}C_s)]_{ver}$ structure always gives the products, H_2 + CH_3 (channel II). On the other hand, channel I results from dynamics initiated over a wide structural region. This difference causes the large branching ratios in favor of channel I.

G. Structures of Excited States of CH_5. The CH_5 radical at the vertical electron capture point has low-lying electronically excited states above the ground-state of CH_5(s-C_s). As shown in the previous section, the ground-state PES in CH_5 is dissociative in nature. To derive information on the PESs for the excited states of CH_5, a preliminary SAC-CI calculation was

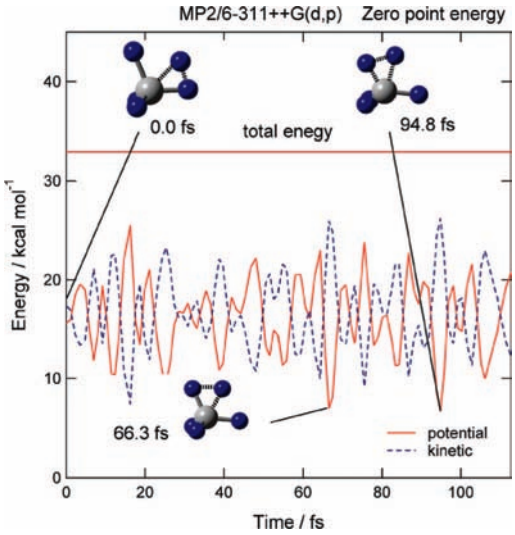

Figure 6. Potential and kinetic energies of CH_5^+ plotted as a function of time, obtained by means of direct ab initio MD calculations. The two components of energy sum to the zero point energy of 32.7 kcal/mol indicated by the horizontal line. Typical snapshots of structures are also shown.

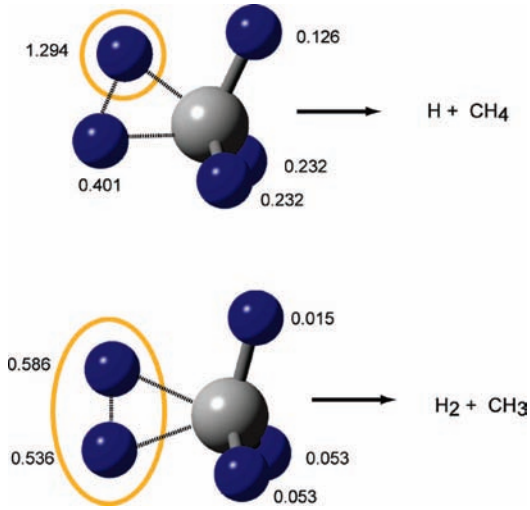

Figure 7. Typical structures of CH_5^+ selected from direct ab initio MD with ZPE. The upper and lower structures give channels I and II after the electron capture, respectively. The values indicate spin densities on the hydrogen atoms of the CH_5 radical at time zero, $[CH_5]_{ver}$.

carried out for the CH_5 radical and the results are given in Table S2 (Supporting Information). The SAC-CI/6-311++G(d,p) calculation for $[CH_5]_{ver}$ shows that the first, second, and third excitation energies are 0.567, 1.802, and 2.168 eV, respectively.

Next, the structures of the first and second excited states were optimized at the SAC-CI/6-311++G(d,p) level. The optimized structures at the first and second excited states are given in the Supporting Information (Figure S4). These excited states were found to be bound and do not fragment to products. The excited-state PESs are thus not dissociative in nature. This result indicates that, following formation by electron capture, internal conversion from the excited states to the ground state may contribute to the dissociation process. Further information on the excited-state PESs is, however, needed to elucidate more details of the excited-state dynamics of CH_5.

4. Discussion

A. Model of Electron Capture Dynamics of CH_5^+. On the basis of the present results, we propose a model for the electron capture dynamics of CH_5^+ which is illustrated schematically in Figure 8. The CH_5^+ ion has a wide Franck−Condon region because of its flexible structure. After the electron capture by CH_5^+, two reaction channels I and II are competitive. If there are two two equivalent hydrogen atoms in the ion that have extended C−H bonds (i.e., the s-C_s type structure), channel II is dominant and the products are $H_2 + CH_3$. On the other hand, if these more extended H atoms are not equivalent, channel I results. The main dissociation route is via channel I, with almost all trajectories following this direction. Channel II is a minor product channel because it occurs from a specific structural configuration of CH_5^+ where the environments of two specific hydrogen atoms are equivalent, such as arises for the s-C_s symmetry structure.

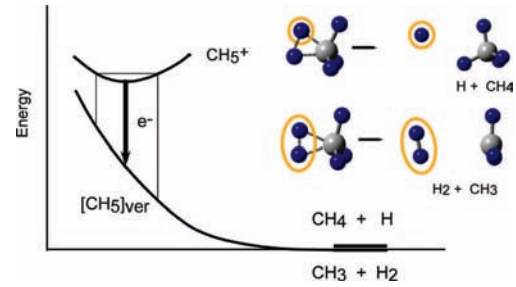

Figure 8. Reaction model of electron capture by CH_5^+ derived from the present study.

B. Comparison with Previous Studies. Previous experiments indicated that both channels I and II are formed following electron capture by CH_5^+ and that the branching ratio to channel II is significantly smaller than that of channel I. Mann et al.[18] determined from their experimental study that the branching ratio of H:H_2 products is 11 (±2):1. From the present calculation, the ratio is obtained to be 13:1, which is in qualitative agreement with the previous experimental results. The CH_5^+ ion has highly fluxional character and the H atoms are exchanged freely by passage over low energy isomerization barriers corresponding to s-C_s and C_{2v} structures (Figure 1).[4,7−18] The present calculation suggests that only specific structures of CH_5^+ (for example, s-C_s symmetry) give channel II. Therefore, the branching ratio to channel II is much smaller than for channel I.

Huang et al.[4] carried out diffusion Monte Carlo calculations of the geometries of the ground-state of CH_5^+ and concluded that the relative probabilities are 38% for the geometry of the e-C_s(I) minimum, 41% at the C_{2v} saddle point, and 22% at the s-C_s(II) saddle point. These population data would suggest that channel II arises from about 22% of the total reactive trajectories because the present study shows that this pathway follows from electron capture at the s-C_s(II) geometry. The present calculations also show, however, that slight deformations from the s-C_s(II) structure result in channel I products. Therefore, the probability of dissociation via channel II becomes significantly smaller than this 22% estimate.

Mann et al.[18] reported product KER distributions for channels I and II. The peaks of the distributions are located around 3.0 eV in both channels. The present calculations support the experimental findings. Channel II also showed a peak at low KER in the experimental data. Unfortunately, the present calculations do not explain this low energy peak because the numbers of trajectories obtained for channel II are too limited, and a much larger number of trajectories must be run for further insights. Recent theoretical investigations have shown, however, that two H−H bond distributions in CH_5 may contribute to the bimodal product KER distributions.[18] The prior observation that

the distribution with shorter H−H bonds is associated with dissociation via channel II is consistent with the present result that the H−H bond distances ($H_1'-H_2'$ in Figure 1) contributing to channel II are close to 1.0 Å.

C. Additional Comments. We have introduced several approximations to calculate regions of the PES and to treat the reaction dynamics. First, we assumed a MP2/6-311++G(d,p) multidimensional PES throughout the dynamics calculations. To check the validity of the MP2 surface, QCISD calculations were carried out for some points obtained in the dynamics simulations, and the energies of the MP2 results were found to be close to those of QCISD calculations (see Supporting Information). Therefore, the MP2 level of theory is judged to be effective to obtain qualitative features of the present reaction dynamics. However, more accurate methods (e.g., CAS and MR-SD methods) may provide deeper insight in the dynamics.

Second, we have assumed that the reaction proceeds on the ground-state potential energy surface of CH_5 and the total energy of the system (4.7 eV) is fixed to the sum of the zero-point energy of CH_5^+ and available energy of $[CH_5]_{ver}$. Any contributions of excited states to the reaction dynamics may change slightly the branching ratio between channels I and II. Surface hopping trajectory calculations may be an effective method to include the coupling effect between ground and excited states.

With the choice of the total energy of the system made in the current calculations, the three-body dissociation channel, $CH_5 \rightarrow CH_3 + H + H$, was not observed. Experimental investigations of the dissociative recombination of $CH_5 + e^-$ carried out in a storage ring have a larger available energy (≥8.0 eV, 185 kcal/mol) than is obtained with the method of electron transfer from C_s atoms used by Mann et al. (4.1 eV, 95 kcal/mol). The DR experiments report the three-body dissociation channel to be dominant,[6] but it is the lower energy experiments that are modeled by the calculations presented here.

In the dynamics calculations, we considered the three low-energy stationary structures of CH_5^+ (e-C_s, s-C_s, and C_{2v}) as initial geometries. The CH_5^+ ion has additional stationary points on the ground-state potential energy surface (for example, structures of C_{4v} and D_{3h} symmetry). The structures and energies of CH_5^+ with the C_{4v} and D_{3h} symmetries are given in the Supporting Information (Figure S5) but are respectively 2.7 and 10.9 kcal/mol higher in energy than e-C_s and have two imaginary frequencies (978 cm^{-1} for C_{4v} and 511 cm^{-1} for D_{3h}). They are not therefore regarded as candidates for dynamically important forms of CH_5^+ in the context of the current dissociative recombination study.

Lastly, in the present study, the initial ranges of structures and momenta of CH_5 are generated from a distribution dictated by the zero-point energy of CH_5^+. This corresponds to a classical distribution. Although CH_5^+ is structurally flexible, the potential energy surface for the dissociation reaction ($CH_4 + H$) is tighter. Quantum effects such as penetration of dissociative wave packets into the walls of the potential, should therefore be small. Modification of the initial conditions to account for quantum mechanical behavior may, however, modify the calculated branching ratios, and thus, to obtain more accurate dynamics, these effects may need to be incorporated. Despite the assumptions summarized above, the results enable us to obtain valuable new information on the mechanism of the electron capture dynamics of CH_5^+.

Acknowledgment. H.T. is indebted to the Computer Center at the Institute for Molecular Science (IMS) for the use of the computing facilities. He also acknowledges partial support from the Daiwa Anglo-Japanese Foundation and a Grant-in-Aid for Scientific Research (C) from the Japan Society for the Promotion of Science (JSPS). A.J.O.E. thanks EPSRC (LASER Portfolio Partnership Grant GR/571750/01) and the Royal Society and Wolfson Foundation for financial support.

Supporting Information Available: Optimized structures, geometrical parameters, and spin densities; time propagations of potential energies, distances, and angles; vibrational frequencies; excitation energies; total energies. This material is available free of charge via the Internet at http://pubs.acs.org.

References and Notes

(1) Belevskii, V. N.; Belopushkin, S. I. *High Energy Chem.* **2005**, *39*, 1.
(2) Iwasaki, M.; Toriyama, K.; Nunome, K. *Radiat. Phys. Chem.,* **1983**, *21*, 147.
(3) White, E. T.; Tang, J.; Oka, T. *Science* **1999**, *284*, 135.
(4) Huang, X. C.; McCoy, A. B.; Bowman, J. M.; Johnson, L. M.; Savage, C.; Dong, F.; Nesbitt, D. J. *Science* **2006**, *311*, 60.
(5) Adams, N. G.; Herd, C. R.; Geoghegan, M.; Smith, D.; Canosa, A.; Gomet, J. C.; Rowe, B. R.; Queffelec, J. L.; Morlais, M. *J. Chem. Phys.* **1991**, *94*, 4852.
(6) Semaniak, J.; Larson, A.; Le Padellec, A.; Stromholm, C.; Larsson, M.; Rosen, S.; Peverall, R.; Danared, H.; Djuric, N.; Dunn, G. H.; Datz, S. *Astrophys. J.* **1998**, *498*, 886.
(7) Müller, H.; Kutzelnigg, W.; Noga, J.; Klopper, W. *J. Chem. Phys.* **1997**, *106*, 1863.
(8) Schreiner, P. R.; Kim, S.-J.; Schaefer, H. F., III; Schleyer, P. v. R. *J. Chem. Phys.* **1993**, *99*, 3716.
(9) Marx, D.; Parrinello, M. *Z. Phys. D* **1997**, *41*, 253.
(10) Marx, D.; Parrinello, M. *Science* **1999**, *284*, 59.
(11) Kumar, P.; Marx, D. *Phys. Chem. Chem. Phys.* **2006**, *8*, 573.
(12) Brown, A.; Braams, B. J.; Christoffel, K.; Jin, Z.; Bowman, J. M. *J. Chem. Phys.* **2003**, *119*, 8790.
(13) Brown, A.; McCoy, A. B.; Braams, B. J.; Jin, Z.; Bowman, J. M. *J. Chem. Phys.* **2004**, *121*, 4105.
(14) McCoy, A. B.; Braams, B. J.; Brown, A.; Huang, X.; Jin, Z.; Bowman, J. M. *J. Phys. Chem. A* **2004**, *108*, 4991.
(15) Jin, Z.; Braams, B. J.; Bowman, J. M. *J. Phys. Chem. A* **2006**, *110*, 1569.
(16) Fleming, F. P.; Barbosa, A. G. H.; Esteves, P. M. *J. Phys. Chem. A* **2006**, *110*, 11903.
(17) Hinkle, C. E.; McCoy, A. B. *J. Phys. Chem. A* **2008**, *112*, 2058.
(18) Mann, J. E.; Xie, Z.; Savee, J. D.; Braams, B. J.; Bowman, J. M.; Continetti, R. E. *J. Am. Chem. Soc.* **2008**, *130*, 3730–3731.
(19) Xie, Z.; Bowman, J. M.; Zhang, X. B. *J. Chem. Phys.* **2006**, *125*, 133120.
(20) Zhang, X.; Braams, B. J.; Bowman, J. M. *J. Chem. Phys.* **2006**, *124*, 021104.
(21) Hickman, A. P.; Miles, R. D.; Hayden, C.; Talbi, D. *A&A* **2005**, *438*, 31–37.
(22) (a) Tachikawa, H. *Phys. Chem. Chem. Phys.* **1999**, *1*, 4925. (b) Tachikawa, H. *Phys. Chem. Chem. Phys.* **2000**, *2*, 4327.
(23) Tachikawa, H. *Phys. Chem. Chem. Phys.* **2008**, *10*, 2200.
(24) Tachikawa, H.; Abe, S. *J. Chem. Phys.* **2007**, *126*, 194310.
(25) Tachikawa, H. *J. Chem. Phys.* **2006**, *125*, 144307.
(26) Tachikawa, H. *J. Chem. Phys.* **2006**, *125*, 133119.
(27) Frisch, M. J.; Trucks, G. W.; Schlegel, H. B.; Scuseria, G. E.; Robb, M. A.; Cheeseman, J. R.; Montgomery, J. A., Jr.; Vreven, T.; Kudin, K. N.; Burant, J. C.; Millam, J. M.; Iyengar, S. S.; Tomasi, J.; Barone, V.; Mennucci, B.; Cossi, M.; Scalmani, G.; Rega, N.; Petersson, G. A.; Nakatsuji, H.; Hada, M.; Ehara, M.; Toyota, K.; Fukuda, R.; Hasegawa, J.; Ishida, M.; Nakajima, T.; Honda, Y. Kitao. O.; Nakai, H.; Klene, M.; Li, X.; Knox, J. E.; Hratchian, H. P.; Cross, J. B.; Bakken, V.; Adamo, C.; Jaramillo, J.; Gomperts, R.; Stratmann, R. E.; Yazyev, O.; Austin, A. J.; Cammi, R.; Pomelli, C.; Ochterski, J. W.; Ayala, P. Y.; Morokuma, K.; Voth, G. A.; Salvador, P.; Dannenberg, J. J.; Zakrzewski, V. G.; Dapprich, S.; Daniels, A. D.; Strain, M. C.; Farkas, O.; Malick, D. K.; Rabuck, A. D.; Raghavachari, K.; Foresman, J. B.; Ortiz, J. V.; Cui, Q.; Baboul, A. G.; Clifford, S.; Cioslowski, J.; Stefanov, B. B.; Liu, G.; Liashenko, A.; Piskorz, P.; Komaromi, I.; Martin, R. L.; Fox, D. J.; Keith, T.; Al-Laham, M. A.; Peng, C. Y.; Nanayakkara, A.; Challacombe, M.; Gill, P. M. W.; Johnson, B.; Chen, W.; Wong, M. W.; Gonzalez, C.; Pople, J. A. *Gaussian 03*, revision B.04; Gaussian, Inc.: Pittsburgh, PA, 2003.

JP806114Y